Construction and Building Materials 82 (2015) 376–390

Contents lists available at ScienceDirect

Construction and Building Materials

journal homepage: www.elsevier.com/locate/conbuildmat

Effect of limestone fillers on microstructure and permeability due to carbonation of cement pastes under controlled CO_2 pressure conditions

Quoc Tri Phung [a,b,*], Norbert Maes [a,1], Diederik Jacques [a,2], Els Bruneel [c,3], Isabel Van Driessche [c,4], Guang Ye [b,d,5], Geert De Schutter [b,6]

[a] Institute for Environment, Health, and Safety, Belgian Nuclear Research Centre (SCK•CEN), Boeretang 200, B2400 Mol, Belgium
[b] Magnel Laboratory for Concrete Research, Department of Structural Engineering, Ghent University, B9052 Ghent, Belgium
[c] Department of Inorganic and Physical Chemistry, SCRiPTS, Ghent University, B9000 Ghent, Belgium
[d] Microlab, Faculty of Civil Engineering and Geosciences, Delft University of Technology, P.O. Box 5048, 2600 GA Delft, The Netherlands

HIGHLIGHTS

- A new carbonation method is proposed considering both advective and diffusive CO_2 transport.
- Portlandite content is gradually decreasing over the depth of sample.
- Limestone fillers can partially play as nucleation sites for precipitation of $CaCO_3$.
- Specific surface area reduces/increases for carbonated sample with/without limestone fillers.
- The carbonation significantly decreases water permeability due to changes in microstructure.

ARTICLE INFO

Article history:
Received 30 October 2014
Received in revised form 27 January 2015
Accepted 11 February 2015

Keywords:
Carbonation
Methodology
Cementitious materials
Permeability
Acceleration
Advection
Diffusion
Characterization
Limestone fillers

ABSTRACT

In underground concrete structures such as radioactive waste disposal facilities, the concrete is subjected to higher CO_2 partial pressure than in the atmosphere and/or higher pressure gradient of liquid in which CO_2 is dissolved. Under these conditions CO_2 transport, which governs the carbonation, occurs both by diffusion and advection. This study aims at developing a new experimental method to carbonate cement-based materials by applying an elevated pressure gradient of pure CO_2 to the specimens at 65% relative humidity (RH). The proposed method was used to investigate the effects of limestone fillers on changes in microstructure and permeability due to carbonation. The experiments were performed on two hardened cement paste samples with different water/powder and limestone filler replacement ratios. Samples were subjected to an elevated CO_2 pressure of 6 bar at the upstream side. The CO_2 uptake was measured in the up- and downstream sides by precise mass flow meters. Carbonated samples were analyzed by a series of methods including SEM, MIP and N_2-adsorption to characterize the microstructural changes; phenolphthalein spraying, XRD, TGA and water permeability measurements to study alterations in chemical compositions and transport properties.

Results showed that the carbonation of samples at 65% RH was considerably fast during the first few experimental hours, while carbonation rate significantly decreased thereafter due to the increase of

* Corresponding author at: Magnel Laboratory for Concrete Research, Department of Structural Engineering, Ghent University, B9052 Ghent, Belgium. Tel.: +32 14 333120; fax: +32 14 323553.

E-mail addresses: QuocTri.Phung@ugent.be (Q.T. Phung), NMaes@sckcen.be (N. Maes), DJacques@sckcen.be (D. Jacques), Els.Bruneel@ugent.be (E. Bruneel), Isabel.VanDriessche@ugent.be (I. Van Driessche), G.Ye@tudelft.nl (G. Ye), Geert.DeSchutter@ugent.be (G. De Schutter).

[1] Tel.: +32 14 333235; fax: +32 14 323553.
[2] Tel.: +32 14 333209; fax: +32 14 323553.
[3] Tel.: +32 92 644447; fax: +32 92 644983.
[4] Tel.: +32 92 64 44 21; fax: +32 92 644983.
[5] Tel.: +31 15 2784001; fax: +31 15 2786383.
[6] Tel.: +32 9 2645521; fax: +32 9 2645845.

http://dx.doi.org/10.1016/j.conbuildmat.2015.02.093
0950-0618/

internal RH. However, by alternating carbonation with drying periods, as proposed here, carbonation rates remained high during the complete experiment. Our study evidenced that, in addition to portlandite, also C–S–H was partly carbonated under the studied conditions resulting in gradual profiles of these phases. Limestone filler replacement promoted the CO_2 uptake because calcite precipitates preferentially on limestone particles than on portlandite and C–S–H phases as the latter inhibits further carbonation. C–S–H carbonation was more enhanced in samples without limestone fillers which resulted in a BET specific surface area increase. On the other hand, in samples with limestone fillers, BET specific surface area decreased because of porosity and pore size decreases. The carbonation induced changes in the microstructure which resulted in a significant decrease in water permeability. As a consequence of larger BET specific surface area, higher porosity and pore size reductions, the decrease in permeability was more pronounced in the sample without limestone fillers.

1. Introduction

Carbonation, initiated when CO_2 penetrates within cement-based materials, is a chemical process of reactions between dissolved carbon species and hydrated cement phases. Carbonation is mainly known as a deterioration phenomenon for reinforced concrete structures because the pH drop [1] leads to higher corrosion rates of reinforcing bars in concrete. On the other hand, carbonation reduces the permeability and porosity [2,3] and increases the mechanical strength of cementitious materials [4]. The carbonated cement-based materials become less permeable; hence transport of hazardous elements is prevented when solidification/stabilization (S/S) in cement-based materials is used for immobilization of hazardous wastes. The carbonation process also changes the geochemical conditions and thus the leaching of the contaminants (e.g. [5]). Recently, carbonation is applied during S/S of heavy metals to improve immobilization. By inducing a slight alkali environment, the solubility of many toxic heavy metals is minimized [6,7]. Furthermore, CO_2 sequestration in cement-based materials seems to be one of the promising methods to cut down CO_2 emissions from industrial sources [8]. In fact, carbon dioxide uptake in cement-based materials can reach 20% by mass of cement [9,10].

The carbonation is a complicated physicochemical process during which CO_2 reacts not only with portlandite but possibly also with other cement hydrates, mainly with the calcium silicate hydrates (C–S–H) [11]. The carbonation process reduces the Ca/Si ratio of C–S–H. It is not easy to distinguish the contribution of portlandite and C–S–H to the overall carbonation because CO_2 simultaneously reacts with portlandite and C–S–H. Borges [12] investigated the contribution of C–S–H carbonation on the formation of calcium carbonates by thermo-gravimetric analysis (TGA) on completely carbonated cement pastes and concluded that the C–S–H carbonation is significantly higher in pastes contained less initial portlandite (high amount of blast-furnace slag replacement). Recently, Morandeau et al. [13] also applied TGA on samples with different carbonation levels (fully-carbonated to non-carbonated state) to study the extent of C–S–H carbonation. More important, they proposed a conceptual model for porosity change by C–S–H carbonation which relates the porosity decrease to the Ca/Si ratio of C–S–H. Those studies were performed under accelerated conditions with high CO_2 concentrations (5% and 10%, respectively) but without advective transport conditions. In this contribution, the methodology for quantifying C–S–H carbonation profiles with thermo-gravimetric analysis is extended to experimental conditions imposing advective transport of pure CO_2.

Under normal conditions, i.e. under low external CO_2 pressure gradients, aqueous or gaseous diffusion of CO_2 in either saturated or partially saturated conditions is the rate-limiting step in the carbonation process [1,10,14] because CO_2 dissolution and reaction rates are much faster. Nevertheless, in the case of concrete used for underground waste disposals, concrete is almost fully saturated and subjected to a high hydrostatic pressure and the surrounding environment may contain a high bicarbonate concentration, for example clay rock in Callovo-Oxfordian formation [15] or Boom clay in Mol site [16]. Furthermore, during the operational period of a repository, a large hydrostatic pressure gradient might build-up because the repositories have not been closed. Therefore, a combination of diffusion and advection should be taken into account when one considers the carbonation mechanism. This is also the case in accelerated carbonation by applying a high pressure gradient in which advection in the gas phase has a significant contribution to the carbonation process. However, so far as the authors are aware, none of the published studies considers the contribution of advection to carbonation of cementitious materials.

In this study, a new method was proposed in which an elevated pressure gradient of pure CO_2 was applied to samples at a controlled internal relative humidity to take into account the contribution of gaseous advection. The method also enables to shorten the experimental time because under atmospheric conditions (low PCO_2, relatively high RH) carbonation is an extremely slow process. A standard way to study the carbonation is to put concrete samples in a controlled chamber with a given CO_2 concentration and optimized relative humidity (50–70%) to speed up the carbonation [17–19]. The drawbacks of such type of experiments are the difficulty in quantification of the CO_2 uptake during carbonation, counting the contribution of pressure gradient and poor in controlling the initial hygrothermal conditions of the samples which are overcome by using the proposed method.

Beside extrinsic factors (e.g. RH, temperature, PCO_2), there are many intrinsic factors influencing carbonation including: water/cement (w/c) ratio, cement type, supplementary cementing materials and limestone filler replacement. Few researchers [17,20] have studied these factors, but many questions still remain, especially about the effects of limestone filler replacement on carbonation. Replacing part of cement by limestone fillers is getting more attention in recent years because of its environmental and economic benefits. Some authors state that concrete with limestone filler replacement leads to an increase in carbonation rate compared to concrete with the same water/powder ratio [21–23]. On the contrary, Tsivilis et al. [24] showed that the carbonation resistance does not decrease even with 35% limestone filler replacement, while Lollini et al. [25] showed a remarkable drop of the carbonation resistance for 30% replacement and no clear effect at 15% replacement.

In the present study, the newly developed carbonation method was applied to investigate the effects of limestone filler replacement on microstructural alterations and permeability changes after carbonation. An integrated analysis of samples with and without limestone fillers at different water/powder ratios before and after carbonation was performed in order to identify how processes at the micro scale are influenced by limestone filler

replacement and eventually effects on transport properties, in particular permeability. The new insights were synthesized in a detailed micro scale conceptual model.

2. Carbonation of cement-based materials under controlled CO_2 pressure gradient

We proposed a new experimental setup which allowed for studying the carbonation under accelerated conditions in which an elevated CO_2 pressure gradient is applied. The setup allowed for easy connecting to other setups before and after carbonation to measure diffusivity [26] or water permeability [27]. The principle was quite simple. An elevated pure CO_2 pressure gradient was applied on a partially saturated sample which was embedded in a special carbonation cell. The penetration of CO_2 into the cement paste sample occurs via two ways: (i) CO_2 gas transports through connected pores under a pressure and concentration gradient, and (ii) dissolved CO_2 transports with the movement of water under a pressure driving force (when initial saturation degree of sample is high). The amounts of CO_2 flowing in and out of the carbonation cell were precisely measured with mass flow meters allowing for quantification of the amount of carbon dioxide reacting with the cement.

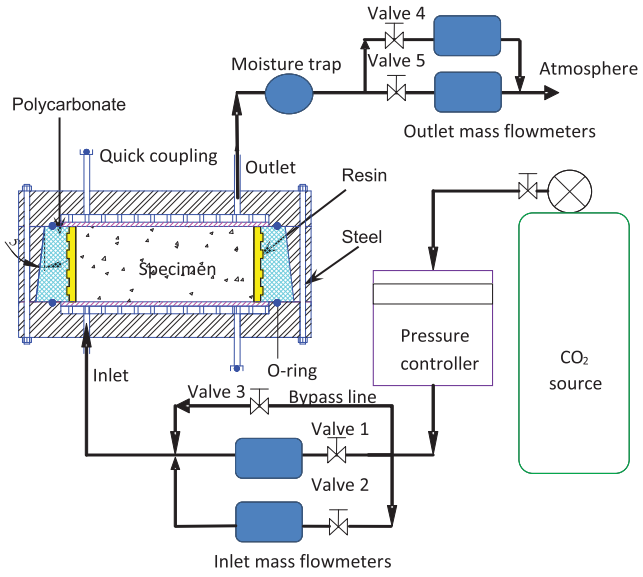

Fig. 1. Proposed carbonation setup using pressurized CO_2 and recording of the CO_2 in- and out-flows.

2.1. Setup for accelerated carbonation

Fig. 1 shows a schematic view of the experimental setup and a picture of the testing rig is shown in Fig. 2. The main part of the system is the carbonation cell which has the same design as the permeability cell described in [27] but with a different embedding procedure (described below). The carbonation cell consisted of two parts: the outer part was made of steel which allowed for applying a high pressure gradient; the inner part was made of polycarbonate to provide a good contact with the resin. The polycarbonate material also enabled a visual check of the contact between the resin and the sample and facilitates further post-mortem analysis. The inner and outer parts fitted together by their conical shapes. The top and bottom lids were also made of steel. The inner surfaces of the lids had a groove network to distribute CO_2 (and water when measuring permeability) evenly on the surface of the sample. Gas tightness was ensured by double O-rings between the lid and the embedded sample. The specimen disk with a diameter of 98 mm and a thickness of 25 mm was embedded into the inner part of the cell by a resin. To prevent leakage around the side of the sample, a resin was chosen with low viscosity, good contact with polycarbonate and cement paste, high strength, transparence and low heat generation during embedding. Sika® Injection-451 was selected as the most optimal choice.

The amount of carbon dioxide reacting with the cement was derived from measurements with two mass flow meters "red-y smart meter GSM" at each side of the carbonation cell. One had a higher measurement range (0–50 ml/min) to measure flow when carbonation rates were high at early experimental times; the other one had a lower range (0–10 ml/min) to measure flow when the carbonation rate was decreased. Using two mass flow meters with different ranges improves the measurement accuracy. The mass flow meters measured every minute the mass flow rate, the total amount CO_2 passing and the temperature. In order to prevent damage of mass flow meters by the high relative humidity conditions, a moisture trap was placed before the outlet mass flow meters. A precise pressure controller (precision of 1/10,000 bar) was used to apply a constant pressure at the upstream side. The other side of the sample was balanced to atmospheric pressure.

2.2. Experimental procedure

Experiments were performed on two sets of hardened cement pastes in a temperature-controlled room of 21 ± 1 °C: sample L0 with water/powder (w/p) ratio of 0.425, 0% of limestone filler replacement; sample L10 with w/p ratio of 0.375 and 10% of limestone filler replacement. The w/c ratio was 0.42 ± 0.05. The

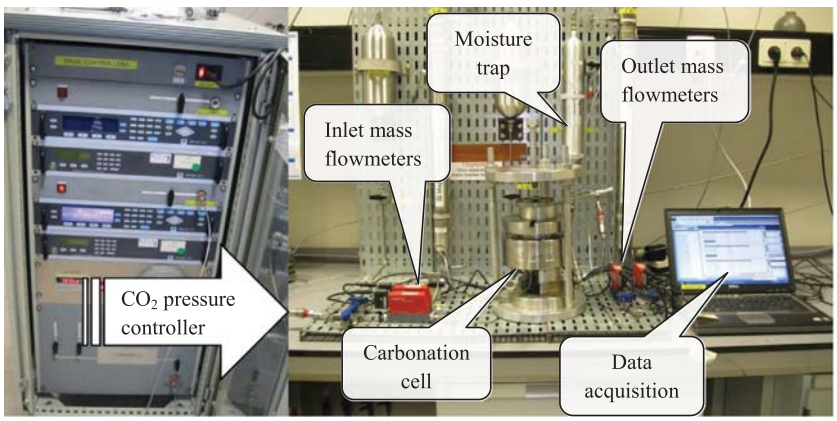

Fig. 2. A picture of the carbonation setup.

carbonated samples are named L0-cont, L10-cont and L10-cyc for continuously-carbonated L0, continuously-carbonated L10 and cyclic-carbonated L10, respectively. Type I ordinary Portland cement (CEM I 52.5 N) was used. The cement has quite high Blaine specific surface of 4350 cm^2/g. Table 1 gives a summary of the chemical properties. Limestone fillers (Calcitec 2001S) has Blaine specific surface of 3500 cm^2/g and $CaCO_3$ content of 98.30%. Other chemical and physical properties are shown in Table 2. Superplasticizer Glenium 27 was added to the mix with content of 0.5% with respect to mass of cement.

Cement paste was poured in a PVC tube with an inner diameter of 98 mm. After 28 days of curing, it was sawn into small disks of 25 mm thick by a diamond saw. Prior to the carbonation experiment, the samples were conditioned to a target internal relative humidity of 65% to have optimal conditions for fast carbonation. To equilibrate the sample to the target RH, we optimized an accelerated conditioning procedure as follows: (i) we estimated the initial RH of the sample (~ 90%) and open porosity (MIP results); (ii) the relationship between porosity, RH, and saturation degree [28,29] was used to estimate the required amount of water evaporation to reach the target RH; (iii) the sample was dried in an oven at 35 °C until the mass decrease approximates the estimated amount of water (4–5 days for RH 65%). An oven temperature of 35 °C prevents cracking and possible dehydration of C–S–H; (iv) the sample was placed into a desiccator containing a certain salt solution ($NaNO_2$) to obtain the target RH until change in mass between two subsequent daily measurements is less than 0.02%. With this procedure, the samples reached the target RH of 65% in a period of less than 1 month.

The sample was then embedded into the inner part of the carbonation cell by a resin within a desiccator at the same RH. It took about 24 h for the resin to dry. The sample was placed in the desiccator for several more days for re-equilibration to the target RH. It is worth noting that embedding before conditioning is not recommended because cracking can occur due to the shrinkage of the restrained sample during the drying shrinkage process.

The carbonation cell was then connected to the CO_2 pressure system at one side while the other side was in contact with air (ambient condition). Prior to the carbonation measurement, the sealing of the whole system was checked to ensure no leakage. All tubes, connections, space were filled up with CO_2 at the high pressure side. These steps are very important because if moisture still remains in the system, the initial RH of the sample can be changed and the quantification of CO_2 uptake is not accurate. We proposed two procedures to carbonate the sample. The first procedure was based on applying a continuous constant CO_2 pressure gradient, the other helped to accelerate the carbonation process by alternating CO_2 application periods with drying periods.

Table 1
Chemical properties (wt.%) of the cement (from manufacturing fact sheet).

CaO	63.0%	Chromium(VI)	$<2{\cdot}10^{-4}$%
SiO_2	20.0%	Cl^-	0.06%
Fe_2O_3	3.0%	Na_2O eq.	0.85%
Al_2O_3	5.0%	Loss on ignition	1.60%
Sulfate SO_3	2.9%	Insoluble residue	0.50%

Table 2
Chemical and physical properties of limestone fillers (from manufacturing fact sheet).

Density	2.7 g/cm^3	$CaCO_3$	98.30%
Blaine specific surface	3500 cm^2/g	MgO	0.36%
Particle size distribution		SiO_2	0.75%
Passing 2 mm	100.0%	Al_2O_3	0.25%
Passing 500 μm	99.9%	Fe_2O_3	0.10%
Passing 125 μm	97.0%	Na_2O eq.	0.05%
Passing 63 μm	77.0%	pH	9.5
D_{50} (50% passing)	10.1 μm		

2.2.1. Continuous carbonation

CO_2 pressure was increased at one side of the sample, while the other side was balanced to atmospheric pressure. At the beginning, the valves connected to inlet mass flow meters (valves 1 and 2 in Fig. 1) were closed, while the valve connected to the bypass line (valve 3) was opened. When pressure reached the target value, valve 1 which was connected to the mass flow meter with high measurement range (up to 50 ml/min) was slowly opened, and then valve 3 was slowly closed. By this way, one avoids damaging the mass flow meter by a sudden increase in flow. The amount of CO_2 going into the system was recorded from the moment valve 1 was opened, which eliminated the amount of gas needed to fill the connections. At the other side of the sample, valve 4 (connected to the low range flow meter) was opened, while valve 5 (connected to the high range flow meter) was closed. In this way, the mass flow meter started measuring the amount of CO_2 leaving the system.

After a few hours of high inlet flow, the inlet flow decreased because the carbonation reaction released water which decreased the air-filled porosity and carbonation products were formed reducing the porosity. When the inlet flow was less than 10 ml/min, the mass flow meter was switched to the low range flow meter.

A constant absolute pressure of 6 bar was applied in order to have at on hand side a sufficient high pressure of pure CO_2 to reduce the experimental time but on the other hand, to reduce the risk for micro cracks in the cement paste sample by applying a too high pressure. A single carbonation test was performed for a period of 4 weeks.

2.2.2. Cyclic carbonation

As the carbonation reaction releases water which increases the local saturation degree and significantly reduces the carbonation rate, carbonation periods were alternated with drying cycles as illustrated in Fig. 3. The sample was first carbonated for time T_1 under the same pressure gradient as applied during the continuous carbonation. Subsequently, it was dried for time T_1' to remove water and bring the sample to a RH which approximates the initial RH (65%). Then a new carbonation – drying cycle started, and so on. The carbonation periods $T_1, T_2, \ldots, T_n$ were determined based on the inlet flow rate. When the rate was less than 0.5 ml/min, carbonation cycle was stopped and the drying cycle starts. The drying periods $T_1', T_2', \ldots, T_n'$ were difficult to determine quantitatively because measurement of the RH within the sample was not possible within this experimental setup. However, trial tests indicated that higher carbonation degree was observed if the drying period increases over time, i.e. $T_1' < T_2' < \cdots < T_n'$. A longer drying period over time reflects a denser cement paste and a deeper carbonation front, resulting in deeper water production, with increasing carbonation. In this study, the cyclic carbonation was only applied on sample L10.

3. Characterization of carbonated materials

After carbonation, a number of post-analysis methods were used to quantitatively and qualitatively analyze the carbonated samples. The carbonated sample was sawn and sprayed by phenolphthalein solution to determine the phenolphthalein carbonation depth [30]. This method only roughly quantifies the zone of carbonation and cannot detect the partly carbonated area with pH values higher than 9 [30,31]. As such, it cannot detect the exact portlandite dissolution front in cementitious systems because the

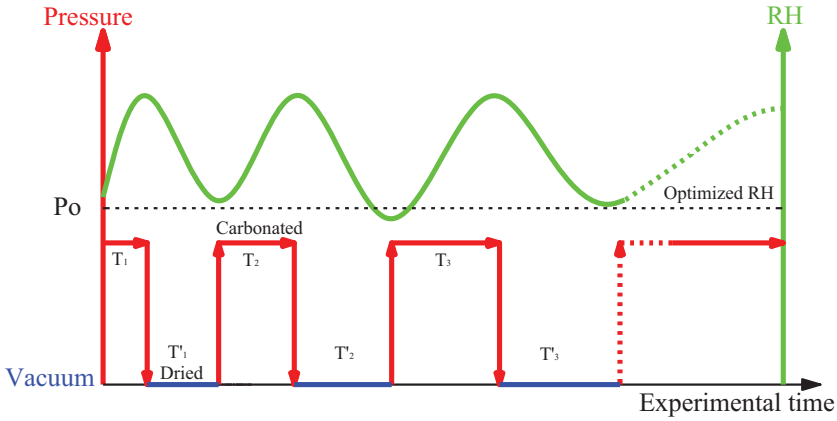

Fig. 3. Schematic illustration of cyclic carbonation procedure to accelerate carbonation process.

pH is buffered at higher values by other cement hydrates [32] resulting in the underestimation of the carbonation depth [33]. To overcome this problem, we determined the portlandite and calcium carbonate profiles of a carbonated sample by thermo-gravimetric analysis of the dust collected at different depths. A hole with a diameter of 10 mm was longitudinally drilled in the carbonated sample. Drilling was halted every 3 mm to collect the dust before continuing drilling. To prevent cross contamination, the hole was carefully cleaned by compressed air before continuing drilling. TGA was performed in a NETZSCH STA 449F3 thermal analyzer. A weighed sample, usually between 30 and 40 mg was heated from room temperature to 1100 °C with a heating rate of 10 °C per minute under a constant nitrogen flow rate of 120 ml/min. A blank test (without sample) was also performed to correct the buoyancy effect which results in apparent mass increases.

XRD was used to identify crystalline phases, mainly the presence of portlandite and calcite. Powder was collected from reference and carbonated sample in another longitudinal drilling with the same procedure as for the TGA. For the carbonated sample, powder was taken from the upstream side up to 3 mm in depth and referred as "carbonated sample". For the reference sample, the surface of sample which might be carbonated by the air was removed before taking the powder. Powder XRD measurements were done using a Philips X'Pert Pro Diffractometer. The samples were scanned over the 2θ range of 5–70° using Cu-Kα radiation at 45 kV and 40 mA.

Mercury intrusion porosimetry, scanning electron microscopy and nitrogen gas adsorption provided information on how pore structure changes during carbonation. Dried samples are required for these techniques. In order to minimize the influence of the drying process on the microstructure, freeze drying was chosen to prepare samples for MIP and nitrogen adsorption measurements. By freeze drying, water crystals sublimate which prevents micro cracks formation because of capillary stress if drying passes through the liquid state [34]. This method also dries the sample in a quite short period. Samples were directly immersed in liquid nitrogen until the escape of gas bubbles stopped. Subsequently, the samples were transferred to a vacuum chamber where a vacuum under 2.5×10^{-2} mbar was applied for 24 h. For SEM measurements, the solvent replacement method was chosen to dry the samples. This method is found to be a good technique to preserve microstructure for SEM analysis [35]. The samples were immersed in 2-propanol 99.5% for 2 weeks, and then placed in a vacuum chamber under 2.5×10^{-2} mbar for 3 days. The dried samples were impregnated in a high strength and extremely low viscosity resin before polishing. The polished samples were then coated by a thin gold layer (few μm) to prevent charging during SEM examination. Even with gold coating, the samples might be charged because a non-conductive resin was used. Therefore, the top and bottom of sample were connected by a conductive copper tape. MIP experiments were performed in a PASCAL 140/440 porosimeter in which the mercury pressure was continuously increased up to a maximum pressure of 200 MPa. Nitrogen adsorption measurements were done on a TriStar II 3020 Micromeritics. SEM measurements of samples were done using a JEOL JSM 6610 scanning electron microscope. Energy Dispersive X-ray analysis (EDX) was carried out with the aid of ESPRIT Software. For MIP and N_2-adsorption, the samples were taken from the upstream side up to 3 mm in depth and referred as "carbonated samples". For SEM, carbonated samples were taken in parallel to the longitudinal axis and scanning area was within 3 mm from the reactive surface. All measurements were also conducted on reference materials.

The effect of carbonation on permeability was quantified with the permeability setup as discussed in [27] on both reference and carbonated samples. The novelty of the permeability setup is that steady-state conditions are controlled by application of a constant flow instead of a constant pressure in standard methods, which overcomes the problem of measuring extremely low flow rate. Furthermore, the permeability setup which is completely compatible with the carbonation setup, can determine the permeability coefficient of cement paste in a relative short time.

4. Results and discussion

4.1. CO_2 uptake

The CO_2 uptake was defined as the ratio between the CO_2 mass which was reacted with the sample and the mass of cement in the sample, expressed as:

$$\text{Uptake}_{CO_2} = \frac{(m_{CO_2}^{\text{inlet}} - m_{CO_2}^{\text{outlet}})}{c} 100\% \quad (1)$$

where $m_{CO_2}^{\text{inlet}}$ and $m_{CO_2}^{\text{outlet}}$ [M] are the mass of CO_2 measured by inlet and outlet mass flow meters, respectively; c is the cement mass in the sample [M]. Fig. 4 shows the CO_2 uptake of L0-cont and L10-cont during 28 days of carbonation. The initial rate of CO_2 uptake was very fast but significantly decreased after a few hours of carbonation. Initially, CO_2 mainly penetrated into the unsaturated (RH = 65%) sample via the gaseous phase. As carbonation proceeded, the released water increased the saturation degree of the sample. At a certain time, the sample was getting saturated close to the inlet which prevented further gaseous transport. Wetter conditions were indeed observed at the upstream side of

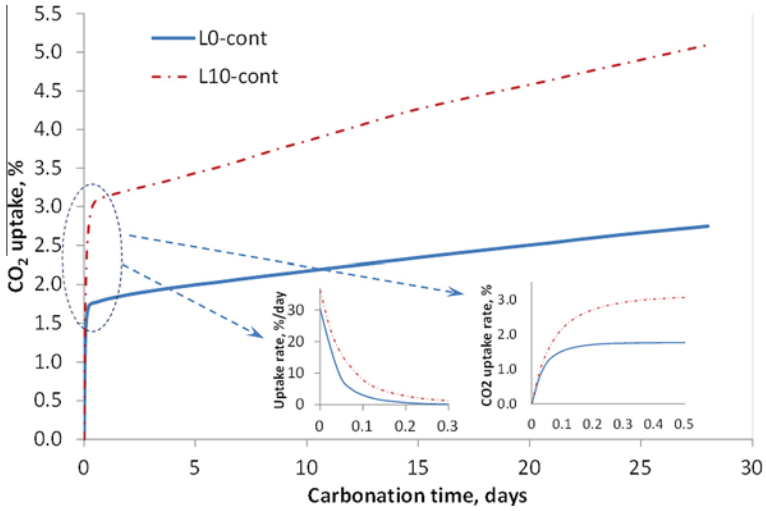

Fig. 4. CO_2 uptake (in percentage wrt. cement mass in sample) of samples L0-cont and L10-cont as a function of time during continuous carbonation – the first derivative curves show a decrease in carbonation rate over time.

the sample. The porosity reduction (showed later) in this layer also contributed to slower CO_2 transport. From the moment of saturation of the first thin layer, the carbonation rate dramatically dropped. The longer the experimental time, the lower the carbonation rate because the released water tended to saturate the entire sample, hence slowing down the CO_2 transport. Both initial and residual CO_2 uptakes were higher for L10-cont than for L0-cont, but major difference was fallen into the initial carbonation stage. This indicates that the CO_2 advection in the gaseous phase during the initial carbonation and diffusion in the aqueous phase after the initial carbonation was higher in L10. Note that the transport of CO_2 is not only affected by the pore structure itself which is represented by "intrinsic" permeability and diffusivity, but also by the hygrothermal conditions (RH, temperature) of the sample. Due to a larger Ca amount and higher potential for C–S–H carbonation (Section 4.3), the reaction rate (between Ca^{2+} and CO_3^{2-}) could be faster for L0-cont. Therefore, the saturation degree was getting higher in the first layer of L0-cont which prevented further CO_2 penetration. Consequently, the saturated water permeability of L0 was even higher than L10 (shown later in Table 6), the transport of CO_2 of L10-cont could be faster than L0-cont because the saturation degree of L0-cont increased quicker than L10-cont. Furthermore, gas permeability may not follow the same trend as water permeability due to slip effects [36] which is affected by internal pore surface area. For sample with limestone fillers, calcite might precipitate preferentially on limestone particles than on portlandite and C–S–H phases (shown later in Fig. 13), which promoted the CO_2 uptake. Additionally, the dilution effect did contribute to larger CO_2 uptake of L10-cont compared L0-cont (i.e. more cement in L0-cont).

Applying cyclic carbonation method significantly increased the carbonation degree as shown in Fig. 5 for L10-cyc. After five carbonation-drying cycles within one week, the CO_2 uptake reached 5.1% which was even larger than the CO_2 uptake after 4 weeks of continuous carbonation. The cyclic carbonation procedure clearly prevented saturation (see Fig. 6), reestablishing gaseous CO_2 pathways and, thereby, high carbonation rates.

4.2. Phenolphthalein test

The carbonation depth determined by phenolphthalein spraying is shown in Fig. 7. It is important to note that the phenolphthalein test does not really measure the carbonation depth but only its pH. The carbonation depth obtained by our carbonation method (coupled diffusion and advection) was not as sharp as the front obtained under diffusive transport conditions such as under natural conditions (low PCO_2, no advection). This observation was supported by TGA results (Section 4.3) in which the portlandite content gradually decreased with distance from the upstream side. The observation of gradual front is due to the mass transport rate of CO_2 is not neglected compared to the reaction rate [37] as it should be under natural conditions. The contribution of advective transport significantly increased the mobility of CO_2, at least in initial carbonation stage. The carbonation depths obtained after 28-days of continuous carbonation were quite similar for L0-cont (2.7 mm) and L10-cont (2.5 mm) despite larger CO_2 uptake of L10-cont. This observation illustrates that the phenolphthalein indicator itself is not a sufficient indicator for carbonation rate. For sample L0-cont, portlandite might still be present but covered in the carbonation product layer while other phases (e.g. C–S–H) were carbonating. Therefore, phenolphthalein spraying led to an overestimation of carbonation depth of L0-cont. The carbonation depth of L10-cyc was twice (5.1 mm) the carbonation depth of L10-cont, even though the carbonation time for the former was only 7 days.

4.3. Mineralogical changes: portlandite and calcium carbonate contents

Fig. 8 presents the XRD patterns for continuous carbonated and reference samples for the first 3 mm from the inlet. Presence of portlandite is indicated by the peaks at $2\theta = 17.9°$ and 34.2°. There was a strong peak at 29.4° corresponding to calcite which was formed during carbonation in both L0-cont and L10-cont. Note that the strong peak of calcite in reference sample L10 is due to the 10% limestone replacement. Interesting is the peak of vaterite in both carbonated L0-cont and L10-cont even with relatively low intensity. The formation of vaterite is favored when the system has a low Ca^{2+}/CO_3^{2-} concentration ratio [38,39] which is the case during accelerated carbonation. Furthermore, the carbonation of ettringite leads to the formation of vaterite crystals [19]. The XRD patterns indicate ettringite dissolution as ettringite peaks were more visible in the reference samples than in the carbonated samples.

Typical thermo-gravimetric and derivative thermo-gravimetric (TG/DTG) curves of L10-cont are shown in Fig. 9. The tangent method was used to determine the percentage of portlandite and calcite in the reference and carbonated samples [40] in order to

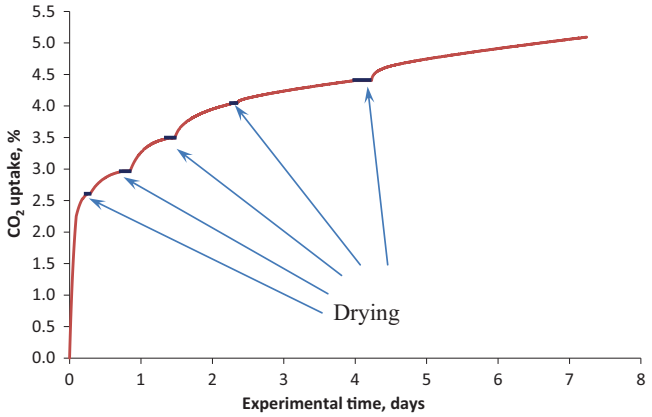

Fig. 5. CO_2 uptake of sample L10-cyc by applying cyclic carbonation method – experimental time referred to the total carbonation and drying time.

take into account the gradual decomposition of C–S–H. The dehydration of C–S–H mainly occurs in temperature range of 180–300 °C [41]. However, it partially decomposes in the other temperature ranges, especially 400–500 °C in which portlandite also decomposes. Two clear steps of portlandite (400–500 °C) and calcite (560–765 °C) decomposition were easy to detect in all samples. However, the formation of vaterite (as found in XRD pattern) during carbonation was not clearly seen.

Fig. 10 shows that in L0-cont and L10-cont, portlandite and calcite, respectively, decreases and increases up to a depth of 12 mm. Note that the surface at the downstream which was not in contact with the pure CO_2 was slightly carbonated by CO_2 originating from the atmosphere (observed at depths above 20 mm). Portlandite was observed in the first sampling interval (0–3 mm) although the phenolphthalein test indicated a pH lower than 9 in that interval (2.7 and 2.5 mm for L0-cont and L10-cont, respectively). It is hypothesized here that under accelerated conditions in which the transport of CO_2 is faster than Ca ions, a calcite layer may form

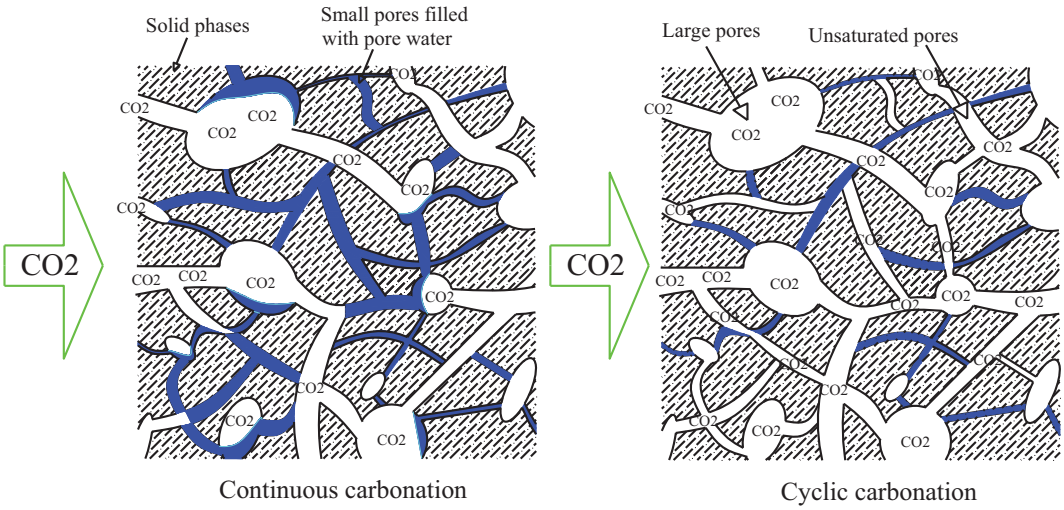

Fig. 6. Conceptual comparison of aqueous and gaseous phase distribution within the cement pore structure during continuous and cyclic carbonation: Saturation degree is significantly increased due to continuous carbonation as small pores are mostly filled with released water as carbonation proceeds; while for cyclic carbonation part of small pores are emptied during drying cycle. Volume of both large and small pores are changed by cyclic carbonation, while mainly large pores for continuous carbonation.

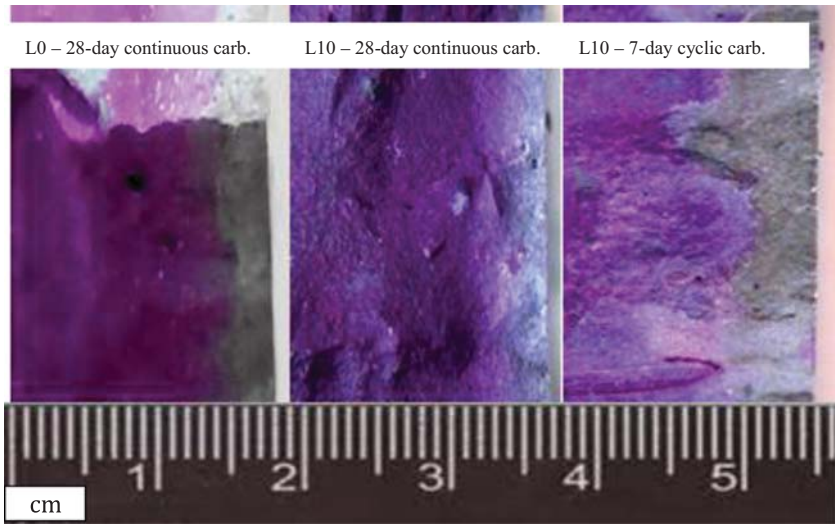

Fig. 7. Carbonation depths of samples L0-cont and L10-cont after 28-day continuous carbonation and of sample L10-cyc after 7-day cyclic carbonation (the carbonated zone is grey colored). (For interpretation of the references to color in this figure legend, the reader is referred to the web version of this article.)

around the portlandite (or C–S–H) particles. Two main consequences are that (i) these portlandite particles are difficult to access for CO_2 and thus further carbonation is prevented (illustrated in Fig. 13), and (ii) the pH of the pore solution is no longer buffered by portlandite.

In order to identify whether other phases (mainly C–S–H) than portlandite react with CO_2, the calculated amount of calcite formed from portlandite was compared with the measured calcite content. The amount of reacted portlandite content was calculated from the difference in portlandite content between the carbonated and reference samples. This value was taken as a proxy for the calcite formed from portlandite carbonation. The calcite formed from C–S–H carbonation (with assumption that the carbonation of the minor phases was negligible) was estimated as the difference between the calcite content measured by TGA and the calcite formed from portlandite. The estimation showed that C–S–H carbonation contributed 41.8%, 33.3% and 4.6% to calcite formation in the intervals 0–3, 3–6 and 6–9 mm for L0, respectively. The carbonation of C–S–H in L10-cont was limited to 15.5% and 6.4% in the intervals 0–3 and 3–6 mm, respectively. There was no C–S–H carbonation observation beyond those depth ranges. Note that the formation of vaterite (as seen in XRD results) is difficult to quantify by TGA, but quantitative XRD would be a relevant method to study the formation of vaterite.

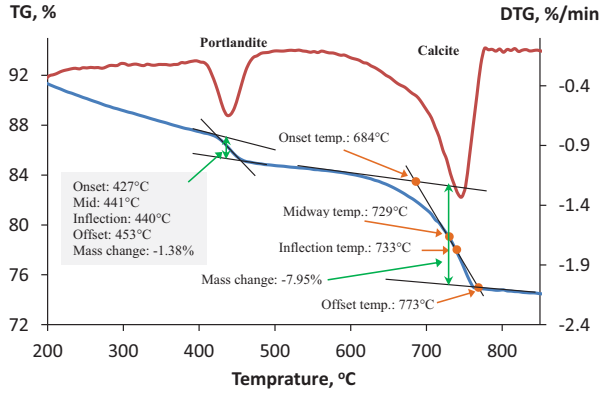

Fig. 9. Illustration of tangent method to determine portlandite and calcite contents of continuously-carbonated sample L10-cont, depth 3–6 mm: TG curve is in blue, DTG curve is in red. (For interpretation of the references to color in this figure legend, the reader is referred to the web version of this article.)

4.4. Microstructural changes: porosity, pore size distribution and specific surface area

4.4.1. MIP results

Table 3 summarizes the MIP results. Note that in this study, the minimum accessible pore was 7.35 nm (corresponding to maximum intrusion pressure of 200 MPa). Continuous carbonation had a larger effect on microstructure for the sample L0-cont than for the sample L10-cont. The porosity of L0-cont was decreased from 16.5% before to 12.9% after continuous carbonation, while L10-cont showed only a slight decrease in porosity from 13.7% to 11.3%. The specific surface area which was calculated based on a cylindrical pore model was decreased by 28% and 14% for L0-cont and L10-cont, respectively. The average pore diameter and median pore diameter (where 50% porosity) were also reduced for continuously-carbonated samples but increased for the sample subjected to cyclic carbonation. Cyclic carbonation increased the porosity in the range 0.04–0.3 μm, but significantly decreased the number of pores smaller than 0.04 μm. The porosity slightly decreased, but the specific surface area significantly reduced from 9.4 m^2/g to 6.8 m^2/g.

The cumulative pore volume and pore size distributions are shown in Fig. 11. When applying continuous carbonation, the threshold pore diameter (at which intruded volume significantly increases) of L0-cont was reduced from 1 μm to 0.1 μm. There was also a reduction in the threshold pore diameter for L10-cont, but it started at lower pore size (reduce from 0.2 μm to 0.06 μm). In contrast, the threshold pore diameter of sample subjected to cyclic carbonation slightly increased, from 0.2 μm to 0.4 μm. Those differences can be attributed to the difference in the w/p ratio of the samples, 0.425 compared to 0.375 for L0 and L10, respectively. Both continuously-carbonated and reference samples had the same critical pore size which is the most frequently occurring pore size in interconnected pores, while it was shifted to larger pore size for cyclic-carbonated sample L10-cyc. The reference samples had a sharp peak which suggests that most of the pores of reference samples mainly distribute in corresponding pore size range while carbonated samples had a rounded peak (even more than one peak for L0-cont) which indicates a broader distribution in pore sizes [42]. The increase in porosity in pore size range 0.05–0.2 μm could be attributed to micro cracking which might occur during process of the cyclic carbonation.

4.4.2. N_2-adsorption results

N_2-adsorption experiments allow for measuring pore sizes smaller than the accessible pore sizes by MIP. The same trend in porosity decrease due to carbonation was observed as for the

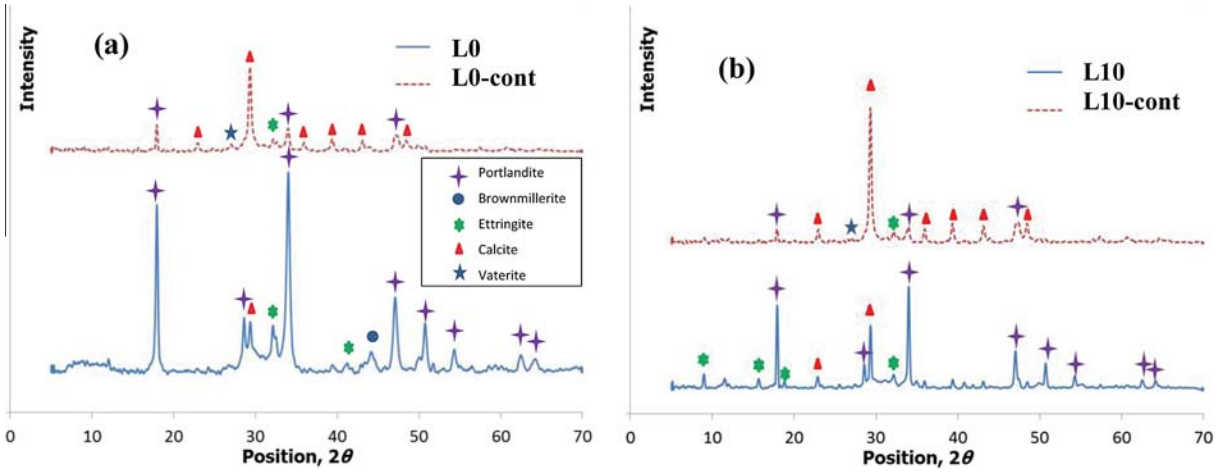

Fig. 8. XRD patterns of reference and continuously-carbonated samples taken in the first 3 mm depth from the inlet: (a) L0 and L0-cont, (b) L10 and L10-cont.

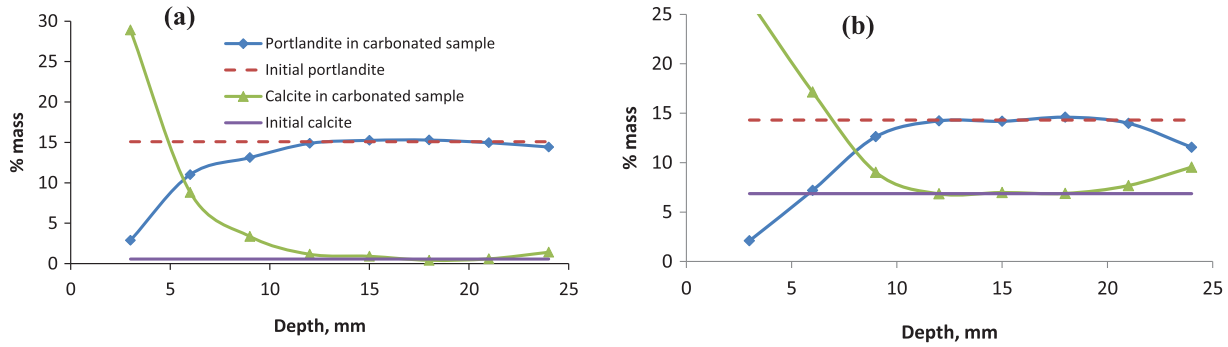

Fig. 10. Changes in portlandite and calcite contents as a function of depth averaged over 3 mm depth intervals of the carbonated samples (a) L0-cont, and (b) L10-cont. The initial portlandite and calcite contents are determined from reference samples.

Table 3
Summary of MIP results of carbonated and reference samples.

Parameters	L0-cont	L0	L10-cont	L10-cyc	L10
Accessible porosity, %	12.9	16.5	11.3	12.8	13.7
Average pore diameter (4V/A), nm	21.8	26.1	21.1	30.2	24.2
Median pore diameter, nm	28.7	32.3	26.9	47.7	32.5
Specific surface, m^2/g	7.7	10.6	8.1	6.8	9.4

Table 4
Summary of N_2-adsorption results of carbonated and reference samples.

Parameters	L0-cont	L0	L10-cont	L10-cyc	L10
BET surface area, m^2/g	38.0	30.6	23.2	13.5	34.1
Porosity (BJH), %	10.7	13.0	8.4	5.1	9.2
BJH adsorption average pore					
Diameter (4V/A), nm	9.7	11.6	9.8	10.3	9.5

MIP results. Carbonation reduced the porosity in all carbonated samples, however, with a larger decrease when cyclic carbonation was applied (at mesopore sizes) as shown in Table 4. Nevertheless, the average pore diameter determined by BJH method remained almost unaltered for L10-cont and even increased for L10-cyc, while a decrease for L0-cont (from 11.6 nm to 9.7 nm) was observed. The micropores (smaller than 2 nm) of sample L10-cyc were also strongly affected by cyclic carbonation. Both micropore surface area and micropore volume were significantly decreased during cyclic carbonation, while effects were less for continuous carbonation (Table 5). As illustrated in Fig. 6, part of the small

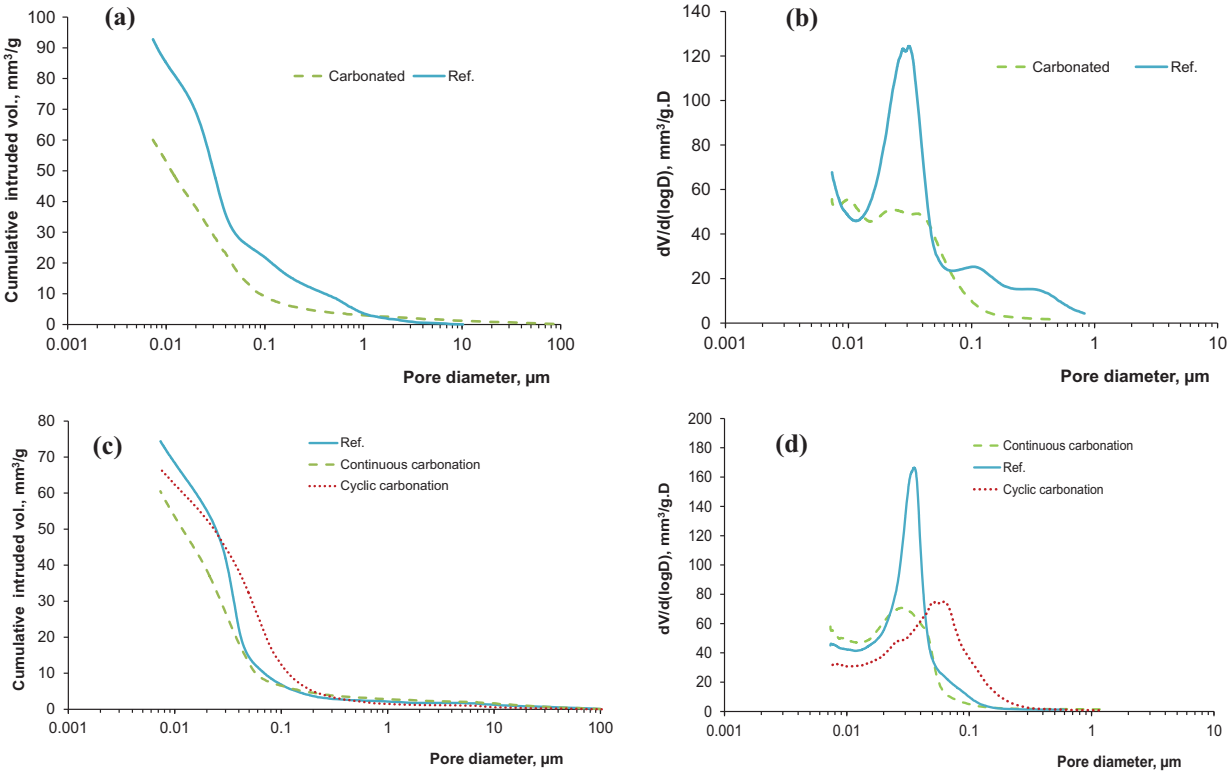

Fig. 11. Changes in pore size distribution (PDS) due to carbonation accessed by MIP: (a) and (b) intruded volume vs. pore diameter and differential PDS of L0 and L0-cont, respectively; (c) and (d) intruded volume vs. pore diameter and differential PDS of L10, L10-cont and L10-cyc, respectively.

Table 5
Micropore information of carbonated and reference samples determined using Dubinin–Astakhov model [52].

Parameters	L0-cont	L0	L10-cont	L10-cyc	L10
Micropore specific surface, m^2/g	28.8	23.7	17.5	10.7	26.4
Micropore volume, mm^3/g	14.1	11.6	8.5	5.3	12.8
Meso/micro volume ratio	4.3	6.9	5.3	5.1	3.9

Table 6
Reduction in permeability of cement pastes after 28-day carbonation.

Sample	L0	L0-cont	L10	L10-cont
Permeability, m/s	2.3×10^{-13}	3.6×10^{-14}	1.4×10^{-13}	4.8×10^{-14}

pores can be emptied during the drying process of cyclic carbonation. Thus, CO_2 can access and react to alter the structure of small pores in terms of surface area and volume fraction.

The relations between specific surface area, average pore size and pore size distribution during carbonation deserve some attention. Most published studies report a decrease in specific surface area after carbonation [43–46]. The decrease is due to both a decrease in total porosity and a shift in the pore size distribution towards smaller pore sizes. The carbonated samples L10-cont and L10-cyc indeed showed a decrease in specific surface area and a decrease in pore volume (Table 4). However, the average pore size distribution did not consistently shift towards smaller pore size range. Therefore, the redistribution in pore sizes and the micropore reduction during carbonation could contribute to the changes in specific surface area instead of only the average pore size decrease. As evidences from micropore information, there was a decrease in both pore volume and specific surface area at nanometer scale of L10-cont and L10-cyc; and the ratio between

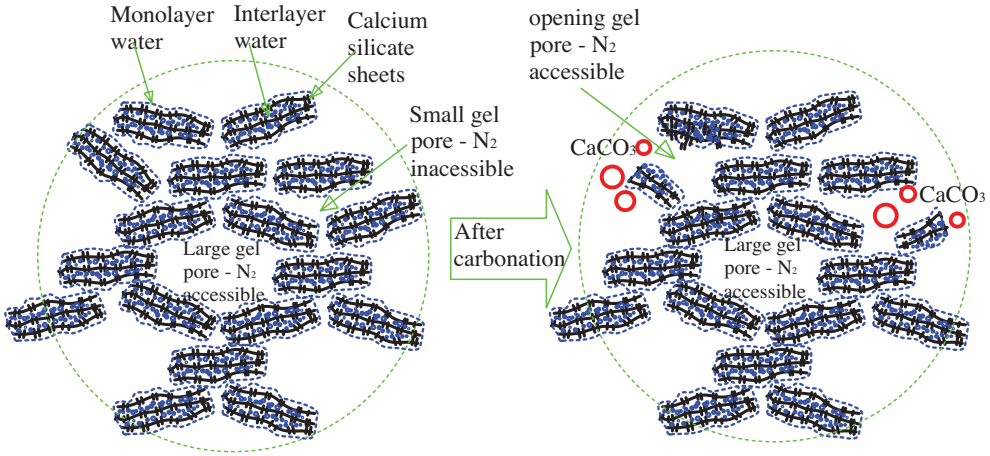

Fig. 12. Schematic illustration of the opening gel pores of C–S–H due to carbonation – C–S–H colloid model adapted from [50].

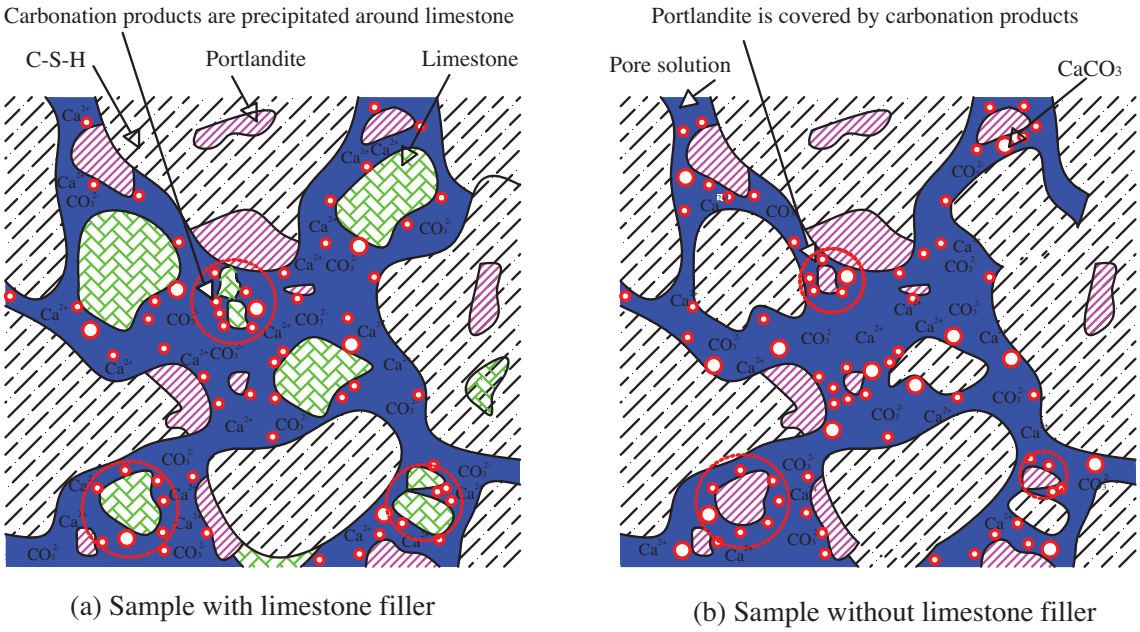

Fig. 13. Effect of limestone fillers on the carbonation – limestone filler plays as a nucleation site for calcium carbonate precipitation.

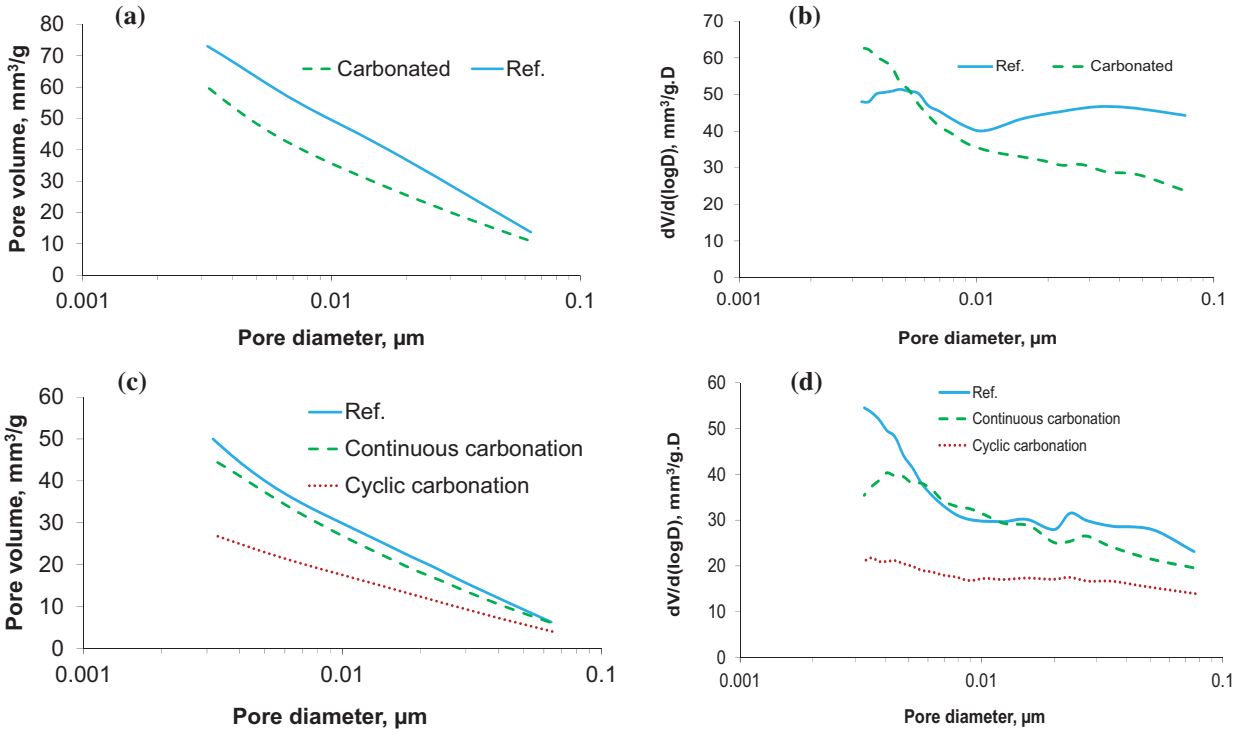

Fig. 14. Changes in pore size distribution due to carbonation accessed by N_2-adsorption: (a) and (b) intruded volume vs. pore diameter and differential pore size distribution (PDS) of samples without limestone filler (L0 and L0-cont), respectively; (c) and (d) intruded volume vs. pore diameter and differential PDS of with 10% limestone filler (L10, L10-cont and L10-cyc), respectively.

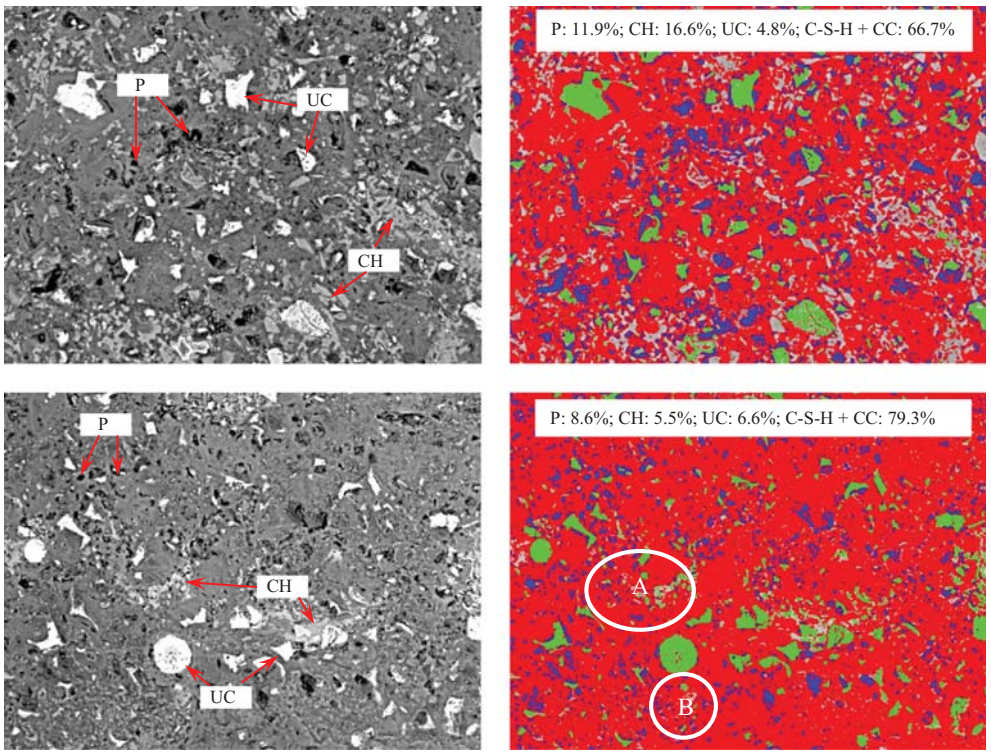

Fig. 15. SEM images (left) and phase segmentation (right) of reference sample L0 (top) and carbonated sample L0-cont (bottom): P = pore (blue), CH = portlandite (grey), UC = unhydrated cement (green), CC = calcium carbonate (red), combined C–S–H and CC (red); field width of 256 µm. (For interpretation of the references to color in this figure legend, the reader is referred to the web version of this article.)

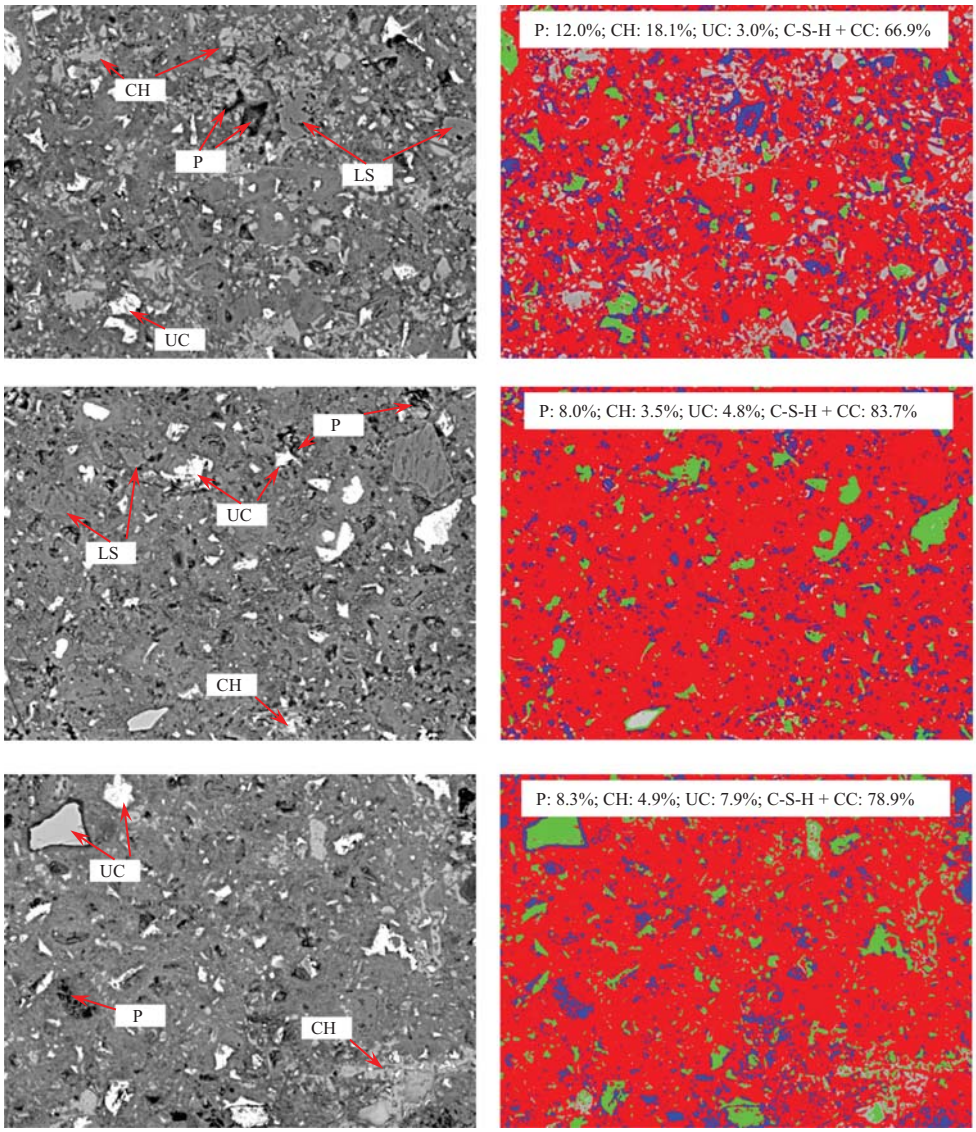

Fig. 16. Comparison of the microstructure and phase fraction of reference sample L10 (top), continuously-carbonated sample L10-cont (middle) and cyclic-carbonated sample L10-cyc (bottom): LS = limestone filler (red), other labels are similar to Fig. 13; field width of 256 μm. (For interpretation of the references to color in this figure legend, the reader is referred to the web version of this article.)

meso/micro pore volumes showed a shift towards higher values after carbonation (Table 5).

On the other hand, it is quite surprising that the BET specific surface area for L0-cont increased from 30.61 m^2/g to 38.02 m^2/g after carbonation. One possible explanation is that the decrease in average pore size is faster than the reduction of total pore volume. This is, however, not supported by the measurements: the porosity decreased 22% and 18% by MIP and N_2-adsorption measurements, respectively, which was similar to the decrease in average pore diameter (27% (MIP) and 16% (N_2-adsorption)). Alternatively, C–S–H gel pores or small necks of ink-bottles pores (narrow entrances but wide bodies) were opening as a consequence of C–S–H carbonation [47]. As indicated by the TGA results, C–S–H carbonation contributed up to 41.8% of calcite formation for sample L0-cont, which was 2.5 times larger than that of sample L10-cont. Both micropore volume and specific surface area were increased as seen in Table 5. This means that the opening of gel pores dominates the changes of micropore structure compared to the pore filling by calcium carbonate precipitation. As the C–S–H carbonation results in its lower Ca/Si ratio, the structure of C–S–H becomes more porous and highly accessible by nitrogen (see Fig. 12). Consequently, the specific surface area is expected to increase [48]. The specific surface area of C–S–H is much higher than the one of bulk paste, for example, low density C–S–H has specific surface area of 250 m^2/g [49] but only part of this contributes to the average specific surface area of sound paste due to limitation in accessibility of nitrogen to small gel pores. It is not clear in many other studies if the reported specific surface area is for samples with or without C–S–H carbonation. For the latter, the difference in specific surface area of carbonated sample L0-cont with findings in literature could be attributed to C–S–H carbonation.

The different alteration of the specific surface area in L0 and L10 during carbonation is due to differences in composition and w/p ratio. The lower w/p ratio of L10 resulted in a lower porosity. The limestone filler also acts as a nucleation site for hydration reactions [51] given a denser sample with a higher hydration degree. Consequently, the accessibility of CO_2 to gel pores is limited compared to sample L0, thereby, lower C–S–H carbonation. In addition, the limestone fillers can also act as nucleation sites for calcite

precipitation from portlandite carbonation. This process then limits the amount of calcite available for forming protecting layers around portlandite particles as schematically shown in Fig. 13. Therefore, the portlandite carbonation is favored compared to C–S–H carbonation for L10.

Fig. 14 presents the pore volume and pore size distribution of carbonated and reference samples determined by BJH method. The L0-cont showed a steeper slope of pore volume at pore diameters smaller than 5 nm which indicates a larger porosity beyond this pore size due to C–S–H carbonation compared to reference sample. However, this larger porosity was not observed on the carbonated samples L10-cont and L10-cyc. A significant porosity decrease was observed for L10-cyc. C–S–H carbonation which results in low density C–S–H might make the carbonated sample L0-cont more accessible to nitrogen.

4.5. Changes in microstructure and phases via SEM

The SEM images in Figs. 15 and 16 allow for comparing the microstructure of the carbonated samples with the reference samples. Backscattered electron images were segmented to distinguish the distribution of portlandite, pores, C–S–H, calcium carbonate and residual cement clinkers based on a grey level histogram. C–S–H and calcium carbonate were difficult to distinguish because of their similarity in brightness intensity. Therefore, C–S–H and calcium carbonate were grouped together. Other minor phases (e.g. ettringite, thaumasite) were not counted in the phase segmentation. The area fraction (equal to volume fraction for isotropic materials) of each phase was calculated and presented on the right-hand sides of Figs. 15 and 16. Note that the porosity calculated from SEM images might be smaller than the real porosity due to limitation of SEM resolution (magnification of 500 in this study). Results showed that carbonation led to a significant decrease in the pore sizes and total porosity which was in line with the results obtained by MIP and N_2-adsorption. The portlandite content was significantly reduced in the carbonated samples. However, L10-cont had higher percentage of portlandite decrease compared to L0-cont. The portlandite carbonation by cyclic method was less than that by continuous method (sample L10). The remaining portlandite was gathered in smaller clusters compared to the reference samples. Furthermore, in carbonated sample without limestone fillers, there were more remaining portlandite located near the pores (area A and B in Fig. 15) which can serve as an evidence for possibility of carbonation products forming around portlandite particles. The total C–S–H and calcium carbonate content increased after carbonation because calcium carbonate was formed and only a small amount of C–S–H was reacted with CO_2. Limestone filler was found in both carbonated and reference sample L10 which had 10% limestone filler replacement. There was no clear trend for the variation of unhydrated cement content.

4.6. Change in water permeability

Permeability (expressed here as hydraulic conductivity) was decreased by a factor of six and three after 4 weeks of carbonation for L0-cont and L10-cont, respectively (Table 6). It is important to mention that permeability should be interpreted as a composite permeability because the carbonation of the sample was not uniform with depth. The permeability decrease was directly linked to the porosity decrease in the carbonated zone. Furthermore, the pore connectivity was probably decreased because of calcite precipitation. In general, mass transport properties are mainly affected by capillary and large pores [53] which are changed by portlandite carbonation but also by the carbonation of C–S–H and other phases contributes to permeability changes. C–S–H carbonation results in calcite precipitation leading to a porosity decrease. However, the molar volume of carbonated C–S–H (lower Ca/Si) would be smaller than uncarbonated C–S–H which increases the porosity [13]. Therefore, in general, the C–S–H carbonation might slightly decrease porosity at nanometer scale as partly supported in Fig. 14 and Table 5 thereby lowering the permeability.

The degree of porosity and average pore diameter reductions were larger for sample L0-cont compared to L10-cont as seen from both MIP and N_2-adsorption results. Furthermore, the C–S–H carbonation increased the surface area as shown by N_2-adsorption results, which reduced the permeability by increasing the friction between the fluid and pore wall. These could be the possible explanations for the higher permeability decrease in L0-cont compared to L10-cont.

5. Conclusions

In this study, a new method was proposed to carbonate partially saturated cement paste samples considering both advective and diffusive CO_2 transport. The proposed method allowed for an accurate quantification of CO_2 uptake, good control of initial conditions and examination of the effect of carbonation on the permeability change of carbonated cement-based materials.

In order to predict the performance of concrete structures in potential enriched CO_2 environments, knowledge of the carbonation rate is needed. The phenolphthalein spraying alone is not an adequate indictor for carbonation rate despite of its common use. The portlandite profile (determined by TGA) combined with CO_2 uptake measurements provide a clear picture of the carbonation degree as illustrated in this study. The CO_2 uptake measurements showed that the carbonation was extremely fast during the first few hours of carbonation when CO_2 transport through the gaseous phase was still dominant. It was then followed by a strong drop in carbonation rate because the sample was gradually saturated by the released water at the upstream part. Cyclic carbonation seemed to be a relevant method to increase the carbonation degree. However, care must be taken in account during drying cycles: too intensive drying could lead to micro cracking occurrence, hence optimization of drying periods is needed. In addition, we can eliminate the cracking by using a rubber ring instead of epoxy resin to embed the sample. This replacement will prevent micro-cracking during drying cycles due to the internal stress generation.

A relative humidity range of 50–70% (which is 65% in this study) is thought to be optimal for carbonation rate providing that the RH slightly varies around the optimal value during carbonation. Nevertheless, in this study the RH can be lower because it is increasing during continuous carbonation. The square-root-time law of carbonation was not applicable under studied conditions indicating the contribution of advective transport. MIP, N_2-adsorption and SEM results confirmed a relative reduction in porosity of the carbonated materials. The pore size distribution of continuously-carbonated samples was slightly shifted to finer pore size range, while larger pore size range for cyclic-carbonated sample. Both continuous and cyclic carbonation resulted in broader pore size distributions compared to reference samples. TGA results showed that portlandite was still present in the carbonated zone detected by phenolphthalein spraying. More important, the portlandite content was gradually decreasing over the depth of sample, while calcite content was gradually increasing which indicates that the carbonation front was not sharp under the condition of coupled advection and diffusion. Portlandite was the main phase which was carbonated but C–S–H could be carbonated under elevated condition, especially in the sample without limestone fillers. The carbonation of C–S–H highly increased the specific surface area due to a process of opening gel pores.

Limestone filler replacement showed some interesting results. The CO_2 uptake was doubled for sample with limestone fillers despite of lower initial water permeability. This is partially attributed to the lower rate of saturation degree increase resulting from lower reaction rate and the precipitation of calcite on limestone particles which promotes CO_2 uptake. Note that under studied conditions the transport rate might not be neglected compared to reaction rate, at least in the initial carbonation stage. Limestone fillers could partially play as nucleation sites for precipitation of calcium carbonates which promoted more portlandite carbonation. The micropore volume and specific surface area were decreased for carbonated sample with limestone fillers, but increased for carbonated sample without limestone fillers as a consequence of C–S–H carbonation.

The carbonation exhibited a significant decrease in water permeability resulting from the changes in microstructure and mineralogy. The permeability decrease could be mainly contributed from portlandite carbonation and partially from C–S–H carbonation.

Acknowledgements

This work is supported by a grant from Belgian Nuclear Research Centre (SCK•CEN). The authors are thankful to Miroslav Honty and Wim Verwimp at SCK•CEN for their help in XRD and N_2-adsorption measurements.

References

[1] Papadakis VG, Vayenas CG, Fardis MN. Fundamental modeling and experimental investigation of concrete carbonation. Aci Mater J 1991;88(4):363–73.
[2] Song HW, Kwon SJ. Permeability characteristics of carbonated concrete considering capillary pore structure. Cement Concrete Res 2007;37(6):909–15.
[3] Claisse PA, El-Sayad H, Shaaban IG. Permeability and pore volume of carbonated concrete. Aci Mater J 1999;96(3):378–81.
[4] Chang CF, Chen JW. Strength and elastic modulus of carbonated concrete. Aci Mater J 2005;102(5):315–21.
[5] Martens E, Jacques D, Van Gerven T, Wang L, Mallants D. Geochemical modeling of leaching of Ca, Mg, Al, and Pb from cementitious waste forms. Cement Concrete Res 2010;40(8):1298–305.
[6] Venhuis MA, Reardon EJ. Carbonation of cementitious wasteforms under supercritical and high pressure subcritical conditions. Environ Technol 2003;24(7):877–87.
[7] Macias A, Kindness A, Glasser FP. Impact of carbon dioxide on the immobilization potential of cemented wastes: chromium. Cement Concrete Res 1997;27(2):215–25.
[8] Barlet-Gouedard V, Rimmele G, Goffe B, Porcherie O. Well technologies for CO_2 geological storage: CO_2-resistant cement. Oil Gas Sci Technol 2007;62(3):325–34.
[9] Ghoshal S, Kashef-Haghighi S. CO_2 sequestration in concrete through accelerated carbonation curing in a flow-through reactor. Ind Eng Chem Res 2010;49(3):1143–9.
[10] Reardon EJ, James BR, Abouchar J. High pressure carbonation of cementitious grout. Cement Concrete Res 1989;19(3):385–99.
[11] Peter MA, Muntean A, Meier SA, Böhm M. Competition of several carbonation reactions in concrete: a parametric study. Cement Concrete Res 2008;38(12):1385–93.
[12] Borges PHR, Costa JO, Milestone NB, Lynsdale CJ, Streatfield RE. Carbonation of CH and C–S–H in composite cement pastes containing high amounts of BFS. Cement Concrete Res 2010;40(2):284–92.
[13] Morandeau A, Thiéry M, Dangla P. Investigation of the carbonation mechanism of CH and C–S–H in terms of kinetics, microstructure changes and moisture properties. Cement Concrete Res 2014;56:153–70.
[14] Papadakis VG, Vayenas CG, Fardis MN. Experimental investigation and mathematical-modeling of the concrete carbonation problem. Chem Eng Sci 1991;46(5–6):1333–8.
[15] Dauzeres A, Le Bescop P, Sardini P, Cau Dit Coumes C. Physico-chemical investigation of clayey/cement-based materials interaction in the context of geological waste disposal: experimental approach and results. Cement Concrete Res 2010;40(8):1327–40.
[16] Craen MD, Wang L, Geet MV, Moors H. Geochemistry of Boom Clay pore water at the Mol site. SCK•CEN-BLG-990 SCK•CEN, Mol, Belgium; 2004.
[17] Atis CD. Accelerated carbonation and testing of concrete made with fly ash. Constr Build Mater 2003;17(3):147–52.
[18] Deceukelaire L, Vannieuwenburg D. Accelerated carbonation of a blast-furnace cement concrete. Cement Concrete Res 1993;23(2):442–52.
[19] Fernández-Carrasco L, Torréns-Martín D, Martínez-Ramírez S. Carbonation of ternary building cementing materials. Cement Concrete Compos 2012;34(10):1180–6.
[20] Lagerblad B. Carbon dioxide uptake during concrete life cycle: state of the art. Swedish Cement and Concrete Research Institute; 2005.
[21] Dhir RK, Limbachiya MC, McCarthy MJ, Chaipanich A. Evaluation of Portland limestone cements for use in concrete construction. Mater Struct 2007;40(5):459–73.
[22] Matthews JD. Performance of limestone filler cement concrete. In: Dhir R, Jones R, editors. Euro-cements: impact of ENV 197 on concrete construction. London, UK: Taylor & Francis; 1994. p. 113–47.
[23] Courard L, Michel F. Limestone fillers cement based composites: effects of blast furnace slags on fresh and hardened properties. Constr Build Mater 2014;51:439–45.
[24] Tsivilis S, Chaniotakis E, Kakali G, Batis G. An analysis of the properties of Portland limestone cements and concrete. Cement Concrete Compos 2002;24(3–4):371–8.
[25] Lollini F, Redaelli E, Bertolini L. Effects of Portland cement replacement with limestone on the properties of hardened concrete. Cement Concrete Compos 2014;46:32–40.
[26] Jacops E, Volckaert G, Maes N, Weetjens E, Govaerts J. Determination of gas diffusion coefficients in saturated porous media: He and CH_4 diffusion in Boom Clay. Appl Clay Sci 2013;83–84:217–23.
[27] Phung QT, Maes N, De Schutter G, Jacques D, Ye G. Determination of water permeability of cementitious materials using a controlled constant flow method. Constr Build Mater 2013;47:1488–96.
[28] van Genuchten MT. A closed-form equation for predicting the hydraulic conductivity of unsaturated soils. Soil Sci Soc Am J 1980;44(5):892–8.
[29] Stora E, Conrardy C, Barbarulo R, Chen J, Thoue F. A reactive transport model based on thermodynamic computations to estimate the atmospheric carbonation of cementitious materials. Rilem Workshop on Long-Term Performance of Cementitious Barriers and Reinforced Concrete in Nuclear Power Plants and Waste Management. 2009;64:193–202.
[30] RILEM. CPC-18 measurement of hardened concrete carbonation depth. Mater Struct 1988;21(6):453–5.
[31] Chang CF, Chen JW. The experimental investigation of concrete carbonation depth. Cement Concrete Res 2006;36(9):1760–7.
[32] de Larrard T, Benboudjema F, Colliat JB, Torrenti JM, Deleruyelle F. Concrete calcium leaching at variable temperature: experimental data and numerical model inverse identification. Comp Mater Sci 2010;49(1):35–45.
[33] Houst YF, Wittmann FH. Depth profiles of carbonates formed during natural carbonation. Cement Concrete Res 2002;32(12):1923–30.
[34] Gallé C. Effect of drying on cement-based materials pore structure as identified by mercury intrusion porosimetry: a comparative study between oven-, vacuum-, and freeze-drying. Cement Concrete Res 2001;31(10):1467–77.
[35] Collier NC, Sharp JH, Milestone NB, Hill J, Godfrey IH. The influence of water removal techniques on the composition and microstructure of hardened cement pastes. Cement Concrete Res 2008;38(6):737–44.
[36] Klinkenberg LJ. The permeability of porous media to liquids and gases. Drilling and Production Practice: American Petroleum Institute; 1941. p. 14.
[37] Ji Y-s, Wu M, Ding B, Liu F, Gao F. The experimental investigation of width of semi-carbonation zone in carbonated concrete. Constr Build Mater 2014;65:67–75.
[38] Kinoshita H, Circhirillo C, SanMartin I, Utton CA, Borges PHR, Lynsdale CJ, et al. Carbonation of composite cements with high mineral admixture content used for radioactive waste encapsulation. Miner Eng 2014;59:107–14.
[39] Han YS, Hadiko G, Fuji M, Takahashi M. Factors affecting the phase and morphology of CaCO3 prepared by a bubbling method. J Eur Ceram Soc 2006;26(4–5):843–7.
[40] Kocaba V. Development and evaluation of methods to follow microstructural development of cementitious systems including slags. EPFL; 2009.
[41] Alarcon-Ruiz L, Platret G, Massieu E, Ehrlacher A. The use of thermal analysis in assessing the effect of temperature on a cement paste. Cement Concrete Res 2005;35(3):609–13.
[42] Diamond S. Reply to the discussion by S. Chatterji of the paper "Mercury porosimetry – an inappropriate method for the measurement of pore size distributions in cement-based materials". Cement Concrete Res 2001;31(11):1659.
[43] Thomas JJ, Hsieh J, Jennings HM. Effect of carbonation on the nitrogen BET surface area of hardened Portland cement paste. Adv Cement Based Mater 1996;3(2):76–80.
[44] Houst YF. The role of moisture in the carbonation of cementitious materials. Int Zeitsch Bauinstand Baudenkmalpflege 1996;2:49–66.
[45] Chen D, Sakai E, Daimon M, Ohba Y. Carbonation of low heat Portland cement paste precured in water for different time. J Univ Sci Technol Beijing Min Metall Material 2007;14(2):178–84.
[46] Johannesson B, Utgenannt P. Microstructural changes caused by carbonation of cement mortar. Cement Concrete Res 2001;31(6):925–31.
[47] Arandigoyen M, Bicer-Simsir B, Alvarez JI, Lange DA. Variation of microstructure with carbonation in lime and blended pastes. Appl. Surface Sci 2006;252(20):7562–71.

[48] Thomas JJ, Chen JJ, Allen AJ, Jennings HM. Effects of decalcification on the microstructure and surface area of cement and tricalcium silicate pastes. Cement Concrete Res 2004;34(12):2297–307.
[49] Thomas JJ, Jennings HM. A colloidal interpretation of chemical aging of the C–S–H gel and its effects on the properties of cement paste. Cement Concrete Res 2006;36(1):30–8.
[50] Jennings HM. Refinements to colloid model of C–S–H in cement: CM-II. Cement Concrete Res 2008;38(3):275–89.
[51] Ramezanianpour AM, Hooton RD. A study on hydration, compressive strength, and porosity of Portland-limestone cement mixes containing SCMs. Cement Concrete Composit 2014;51:1–13.
[52] Dubinin MM, Astakhov VA. Description of adsorption equilibria of vapors on zeolites over wide ranges of temperature and pressure. Molecular Sieve Zeolites-II: American Chemical Society; 1971. p. 69–85.
[53] Perlot C, Verdier J, Carcasses M. Influence of cement type on transport properties and chemical degradation: application to nuclear waste storage. Mater Struct 2006;39(5):511–23.